ISSN 1063-7842, Technical Physics, 2008, Vol. 53, No. 10, pp. 1336–1343. © Pleiades Publishing, Ltd., 2008.
Original Russian Text © V.I. Balakshii, V.B. Voloshinov, G.A. Knyazev, L.A. Kulakova, 2008, published in Zhurnal Tekhnicheskoĭ Fiziki, 2008, Vol. 78, No. 10, pp. 87–95.

ACOUSTICS, ACOUSTOELECTRONICS

Investigation into the Acoustooptic Properties of Tellurium Crystals by Anisotropic Diffraction of Light

V. I. Balakshii[a], V. B. Voloshinov[a], G. A. Knyazev[a], and L. A. Kulakova[b]

[a] *Moscow State University, Moscow, 119991 Russia*
e-mail: volosh@phys.msu.ru

[b] *Ioffe Physico-Technical Institute, Russian Academy of Sciences, Politekhnicheskaya ul. 26, St. Petersburg, 194021 Russia*

Received January 23, 2008

Abstract—The optical, acoustic, and acoustooptic properties of tellurium crystals viewed as a candidate material for mid- and far-IR acoustooptic devices are considered. The phase velocities, polarization, and drift angles of the acoustic energy in different crystal planes are calculated. The acoustooptic figure of merit for tellurium under the anisotropic diffraction conditions is estimated, and light–sound interaction geometries promising for acoustooptic applications are discussed. Measuring data for the optical and acoustooptic parameters of tellurium crystals are given.

PACS numbers: 78.20.Hp, 42.70.Km, 42.79.Jq

DOI: 10.1134/S1063784208100137

INTRODUCTION

Light–sound interaction is finding application in various areas of science and technology, such as optics, acoustics, optoelectronics, and optical data processing. Specifically, diffraction of light by acoustic waves is widely used for controlling optical radiation characteristics [1–3]. Acoustooptic modulators, deflectors, and filters offer wide functionality, reliability, ease of electronic control, and low energy consumption [1–5]. Therefore, acoustooptic devices are used to advantage in optics and spectroscopy, laser technology and optical communication, medicine, environmental monitoring, astronomy, etc. They can operate in the UV, visible, near-IR, and mid-IR ranges of the spectrum [1–5]. In most acoustooptic devices, paratellurite (TeO_2) crystals are used. This material has a high figure of merit, $M_2 = 1.2 \times 10^{-15}$ s^3/g, and the driving electric signal power in TeO_2-based devices is therefore fairly low. Unfortunately, paratellurite is transparent in the wavelength range 0.35–5.00 μm and hence inapplicable for the mid- and far-IR ranges (λ = 5–20 μm) [1–6].

Efficient acoustooptic devices intended for the mid- and far-IR ranges have not been developed to date. The basic difficulty here is that the diffraction efficiency varies in inverse proportion to the wavelength squared [1–5]. Analysis shows that, to provide the operating efficiency in the mid- and far-IR ranges as high as that provided by paratellurite in visible light, it is necessary to use materials with figure of merit $M_2 = 100 \times 10^{-15}$ s^3/g.

Today, the list of acoustooptic crystals appropriate for use in the far infrared is limited by germanium, TAS (Tl_3AsSe_3), calomel (Hg_2Cl_2), mercury bromide (Hg_2Br_2), and tellurium [5–12]. They all, except for tellurium, have a comparatively low figure of merit, $M_2 = 4.5 \times 10^{-15}$ s^3/g [1–5]. Of them, only TAS and calomel single crystals were applied in acoustooptic devices that carry out spectral filtering of radiation and image processing in the far infrared [9–11]. However, their performance in the far infrared turned out to be inferior to that of paratellurite in the visible and near-IR ranges. The main reason is a low acoustooptic figure of merit of crystals designed for the infrared.

As follows from publications, single-crystalline tellurium is a promising medium for acoustooptic interaction in the mid- and far-IR ranges. Tellurium is of interest because of its extremely high acoustooptic figure of merit, $M_2 > 500 \times 10^{-15}$ s^3/g [12]. However, despite tellurium having been long viewed as an acoustooptic material, its efficiency in acoustooptic devices (deflectors or filters) has yet to be proved. It is known that, in acoustooptic scanners and filters, it is reasonable to apply anisotropic Bragg diffraction, which features optical mode changeover [1–4]. The aim of this work was to study the optical, acoustic, and acoustooptic properties of tellurium single crystals under the conditions of anisotropic diffraction to see whether this material can be used in deflectors and wide-aperture filters.

1. PHYSICAL PROPERTIES OF TELLURIUM CRYSTALS

Tellurium single crystals belong to the 32(D_3) class of the trigonal system [1–6, 12–26]. The melting point and density of the material are, respectively, 452°C and 6.25 g/cm^3. The triad axis, i.e., the C or Z axis, which is a basic symmetry element, coincides with the optical axis. There are also three equivalent dyad axes, X_1, X_2,

and X_3, which make an angle of 120° with each other. Tellurium has left-handed, D_3^4, and right-handed, D_3^6, modifications [18–26]. The former was investigated in this work.

Tellurium is transparent in the IR range of the spectrum (λ = 4–20 μm) [12–14]. Its optical properties differ from those of most acoustooptic materials [1–9]. For example, the refractive indices of the tellurium crystal at wavelength λ = 10.6 μm for the ordinary and extraordinary modes are, respectively, n_o = 4.8 and n_e = 6.25. This means that the birefringence of the crystal is large, $\Delta n = n_e - n_o = 1.45$ [13, 14]. High refractive indices cause a high Fresnel reflection of optical waves. As follows from calculations, the power reflection coefficients are R = 43 and 52% for the ordinary and extraordinary waves, respectively. Therefore, tellurium-based acoustooptic cells must have antireflection coatings. Additional problems are associated with large Brewster angles, 81° and 78°, and small angles of total internal reflection, 9.2° and 12° for ordinary and extraordinary waves, respectively. Finally, tellurium has a low transparency, especially for extraordinary optical waves [13, 14]. This feature can be considered as the primary disadvantage of the material.

Crystalline tellurium belongs to the symmetry group 32, which means the presence of six independent coefficients c_{ij} in the elasticity tensor, which completely determine the acoustic properties of the material. In this work, their values were taken to be $c_{11} = 37.6 \times 10^{10}$, $c_{12} = 9.4 \times 10^{10}$, $c_{13} = 28.8 \times 10^{10}$, $c_{14} = +14.3 \times 10^{10}$, $c_{33} = 78.5 \times 10^{10}$, and $c_{44} = 35.5 \times 10^{10}$ dyn/cm^2 [27]. It should be noted that coefficient c_{14} in the tellurium samples studied was positive and relatively large. The positiveness of this coefficient is characteristic of the left-handed modification of the crystal, and a large value of c_{14} indicates a weak symmetry of the material [20].

2. PROPAGATION OF ACOUSTIC WAVES IN TELLURIUM

The acoustic properties of the crystal were determined by the standard technique using the Christoffel equation and known values of elasticity tensor components c_{ij} [25–27]. We also calculated the phase velocities of three possible acoustic modes for each direction of acoustic wave normal **m**. In addition, drift angle α, as well as the directions of ray vector **s** and polarization vector **r**, were found.

The directions of the phase velocity vector and acoustic wave normal were specified in orthogonal coordinate system (X, Y, Z) with azimuthal angle φ_a measured in the XY plane from the X axis and polar angle θ_a measured from the Z axis. The components of unit vector **m** are then written in the form

$$m_1 = \cos\varphi_a \sin\theta_a; \quad m_2 = \sin\varphi_a \sin\theta_a; \quad m_3 = \cos\theta_a. \tag{1}$$

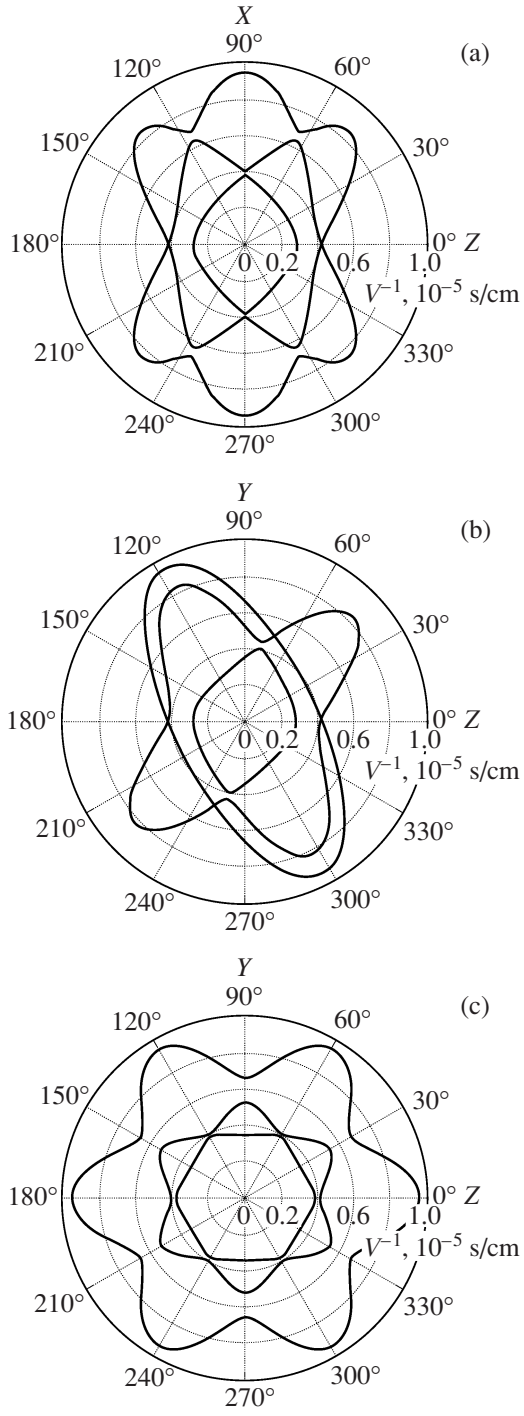

Fig. 1. Cuts of the acoustic slowness surfaces made by the (a) XZ, (b) YZ, and (c) XY planes.

Figure 1 shows the sound speed calculated for three main crystal planes of crystalline tellurium. Polar angle θ_a is measured from the Z axis counterclockwise, and inverse velocity (acoustic slowness) $1/V$ is measured along the radius. The slow shear mode is of most interest in designing acoustooptic devices, since acoustooptic figure of merit M_2 is inversely proportional to V^3. Moreover,

it is shear waves, as a rule, that make it possible to realize anisotropic diffraction in crystals [1–5].

The cut made by the *XZ* plane of the crystal in the acoustic slowness surface is demonstrated in Fig. 1a. The planes rotated through angles $\varphi_a = 60°$, 120°, and 180° about the *Z* axis leave the same sections. As follows from this figure, the lowest speed is observed when the wave propagates along the *X* axis. This wave is a purely shear mode with velocity $V_s = 1.05 \times 10^5$ cm/s, and its polarization vector *r* is directed at an angle of –63° to the *Z* axis in the *YZ* plane. Two other acoustic modes are also "pure": the fast purely shear mode and purely longitudinal mode travel with velocities $V_s = 2.61 \times 10^5$ and $V_l = 2.45 \times 10^5$ cm/s. For all these modes, drift angle $\alpha = 0$. Acoustic waves traveling along the *Z* axis are of minor significance in designing deflectors and filters, since they are rather fast. For example, the purely longitudinal mode propagates along the *Z* axis with velocity $V_l = 3.54 \times 10^5$ cm/s and the velocity of the purely shear mode polarized in the *XY* plane is $V_s = 2.38 \times 10^5$ cm/s.

Figure 1b shows the cut of the acoustic slowness surface made by the *YZ* plane of the crystal. The *Y* axis is not a symmetry plane in this crystal [25, 26]. Nevertheless, the slow shear acoustic wave propagating along the *Y* axis is a pure mode. Its velocity is $V_s = 1.5 \times 10^5$ cm/s, and its displacement vector is aligned with the *X* axis. Two other acoustic waves along the *Y* axis are a quasi-shear mode with velocity $V_{qs} = 1.89 \times 10^5$ cm/s and a quasi-longitudinal mode with velocity $V_{ql} = 2.85 \times 10^5$ cm/s, both polarized in the *YZ* plane. The acoustic walk off angles for these waves are, respectively, 45°, 49°, and 38°.

The minimal sound speed in the *YZ* plane, $V_s = 1.05 \times 10^5$ cm/s, is observed for the purely shear acoustic wave propagating at angle $\theta_a = 116.5°$ with its polarization vector aligned with the *X* axis. This wave is of interest not only because it has the lowest velocity but also because it remains a purely shear wave polarized along the *X* axis irrespective of angle of propagation θ_a. This means that the electric energy applied to a piezoelectric transducer can be entirely converted to the energy of a single elastic wave. Calculations show that this wave features a strong drift of acoustic energy. For example, drift angle $\alpha = 0$ at $\theta_a = 116.5°$ and increases with θ_a, reaching a maximum, $\alpha = 46°$, at $\theta_a = 139°$.

Since the *Z* axis in tellurium is the triad axis, the dependence of the acoustic slowness on angle φ_a has a period of 120°. Moreover, the φ_a dependence of the acoustic slowness has period $\Delta\varphi_a = 60°$ in the *XY* plane (the patterns are mirror-symmetric about the *Z* axis, Fig. 1c).

The angular dependences of the acoustic slowness in three mutually orthogonal planes of tellurium depicted in Fig. 1 give a general pattern of acoustic wave propagation in the crystal. From these dependences, one can choose an acoustic mode and crystal cut that are optimal for designing modulators, deflectors, or filters.

3. ACOUSTOOPTIC FIGURE OF MERIT OF TELLURIUM

The calculated values of acoustic velocities *V* were used to determine the acoustooptic figure of merit of the material. Due to the photoelastic effect, the acoustic wave creates a phase diffraction grating in the crystal. The photoelastic effect is meant as change $\Delta\varepsilon_{il}$ in the permittivity tensor under the action of acoustic strain S_{ij},

$$\Delta\varepsilon_{il} = -\varepsilon_{ij} p_{jkmn} \varepsilon_{kl} S_{nm}, \quad (2)$$

where p_{ijkl} are the components of fourth-order photoelasticity tensor $\hat{\mathbf{p}}$ [1–6, 25] and ε_{ij} are the components of the permittivity tensor. The components of the photoelasticity tensor are usually written in the matrix form as $p_{\alpha\beta}$, where $\alpha, \beta = 1, 2, \ldots, 6$. When calculating the acoustooptic figure of merit for tellurium, the values of $p_{\alpha\beta}$ for crystalline tellurium were taken from [21]: $p_{11} = 0.164$, $p_{12} = 0.138$, $p_{13} = 0.146$, $p_{14} = -0.040$, $p_{21} = 0.138$, $p_{31} = -0.086$, $p_{33} = 0.038$, $p_{41} = 0.280$, $p_{44} = 0.140$, and $p_{66} = 0.013$. The components of the strain tensor are determined using the eigenvalues of displacement vector **u** found by solving the Christoffel equation,

$$S_{ij} = \sqrt{\frac{2P_a}{\rho V^3 lb}} \frac{r_i m_j + r_j m_i}{2}, \quad (3)$$

where P_a is the acoustic wave power and *l* and *b* are the geometrical sizes of the acoustic beam cross section (*l* is the length of the acoustic beam in the plane of acoustooptic interaction).

With the Bragg matching condition fulfilled, diffraction efficiency ζ is given by

$$\zeta = \sin^2\left(\frac{\pi}{\lambda}\sqrt{\frac{l_0 l_1}{2lb}} M_2 P_a\right). \quad (4)$$

Thus, the diffraction efficiency depends on acoustooptic figure of merit M_2, acoustic wave power P_a, cross-sectional area of the acoustic column, and lengths $l_0 = l/\cos\theta_0$ and $l_1 = l/\cos\theta_1$. Lengths l_0 and l_1 depend on the angle of incidence of light on the acoustic wave front, θ_0, and angle of diffraction θ_1. They determine the path length of optical beams of the first and zeroth diffraction orders in the acoustic column [1]. These angles are found from the Bragg condition, which, in the vector form, is written as [1–4]

$$\mathbf{k}_1 = \mathbf{k}_0 \pm \mathbf{K}, \quad (5)$$

where $k_0 = 2\pi n_0/\lambda$ and $k_1 = 2\pi n_1/\lambda$ are the wavenumbers for the incident and diffracted light, n_0 and n_1 are the respective refractive indices, and $K = 2\pi f/V$ is the wavenumber of ultrasound. Having chosen angle of incidence θ_0, one can calculate diffraction angle θ_1 and

acoustic frequency f that meets matching condition (5). Then, the acoustooptic figure of merit can be calculated provided that the directions of polarization unit vectors $\mathbf{e}^{(0)}$ and $\mathbf{e}^{(1)}$ in the first and zeroth orders of diffraction are known.

Acoustooptic figure of merit M_2 can be found using formula (3),

$$M_2 = \frac{1}{4n_0 n_1 \rho V^3} \times [e_i^{(1)} \varepsilon_{ij} \varepsilon_{kl} e_l^{(0)} p_{jkmn} (r_m m_n + r_n m_m)]^2. \quad (6)$$

In tellurium-based wide-aperture filters, light propagation angles θ_0 and θ_1 are large; therefore, it is necessary to take into consideration the difference of lengths l_0 and l_1 from l. The orthogonal approximation is valid only for modulators and deflectors, in which angles θ_0 and θ_1 are small.

4. ACOUSTOOPTIC EFFECT IN TELLURIUM

Anisotropic acoustooptic interaction in crystalline tellurium was investigated with a dedicated computer program. The phase and group velocities, drift angles, and directions of acoustic wave polarization were determined. From the acoustic data, frequency dependences of Bragg angles of incidence for all possible directions of light and sound propagation were determined. The refractive indices for the ordinary and extraordinary optical beams and their polarization vectors were included in the calculation. The ultimate goal of calculation was to find acoustooptic figure of merit M_2 for given conditions of anisotropic diffraction.

Below, we present computational results that may be of value in designing acoustooptic deflectors and filters. The calculation was carried out for wavelength $\lambda = 10.6$ μm. The emphasis was on diffraction of light by a slow shear wave, since this acoustic mode allows achievement of a very high acoustooptic figure of merit.

4.1. Acoustooptic Interaction in the XZ Plane

It turned out that the crystal offers a high acoustooptic figure of merit if acoustic waves propagate in the *XZ* plane. For example, acoustooptic devices may employ a slow shear wave excited along the *X* direction, as illustrated in Fig. 2, which illustrates the spatial pattern of the acoustooptic effect in tellurium, i.e., the distribution of M_2 (in units of 10^{-15} s^3/g) for different directions of incident light. In Fig. 2, the direction of light beams is set by azimuthal angle φ_o and polar angle θ_o (the latter, as in the case of acoustic waves, is counted from the *X, Y,* and *Z* axes). Ultrasound propagates in the crystal at angles $\varphi_a = 0°$ and $\theta_a = 90°$ (point *A* in Fig. 2). The calculation was performed for φ_o varying from 0° to 90° and θ_o varying from 0° to 180°. To set specific values of angles φ_o and θ_o, the mutual orientation of the optical, **k**, and acoustic, **K**, wave vectors should be taken into account. Obviously, keeping the direction of sound propagation the same and varying Bragg angles of incidence, one can set up different conditions of anisotropic diffraction [1–4].

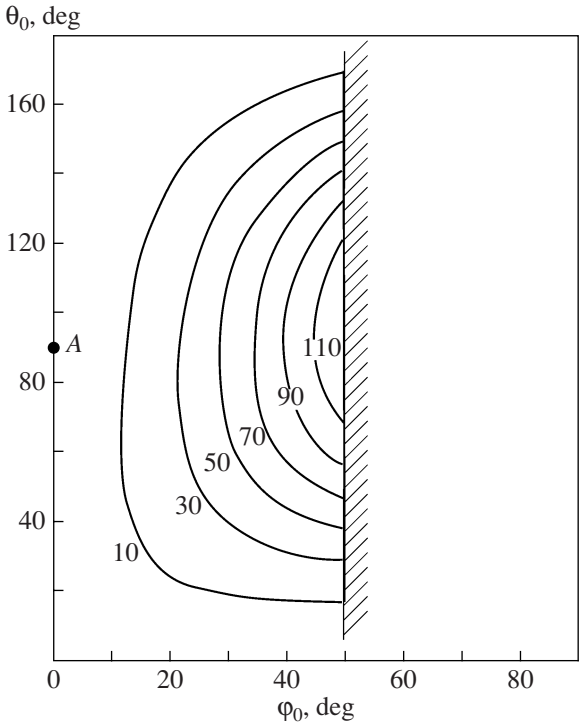

Fig. 2. Acoustooptic figure of merit in the *XZ* plane for ultrasound propagating at angle $\theta_a = 90°$.

The diagram in Fig. 2 corresponds to the low-frequency branch of anisotropic diffraction [1–3]. The high-frequency one is of less interest, since sound at a frequency of several hundred megahertz strongly decays, propagating in the crystal. The calculation shows that acoustooptic figure of merit M_2 reaches a maximum of 130×10^{-15} s^3/g when the shear wave travels along the *X* axis, i.e., when the extraordinary wave propagates at angles $\varphi_o = 50°$ and $\theta_o = 96°$. In the dashed domain at $\varphi_o > 50°$, acoustooptic interaction is absent, since Bragg matching condition (5) is violated here. The above statement is illustrated in Fig. 3, where Bragg angle θ_B is plotted against ultrasonic frequency f for the ordinary (curve *o*) and extraordinary (curve *e*) waves and also against acoustooptic figure of merit M_2. In the *XZ* plane, parameter M_2 reaches a maximum near ultrasonic frequency $f = 400$ MHz at a minimal value of Bragg angle of 40° for the extraordinarily polarized light. In this case, the Bragg angle for the ordinarily polarized light equals zero. Clearly, such a geometry of acoustooptic interaction is of practical interest, since it is optimal for acoustooptic deflectors and modulators.

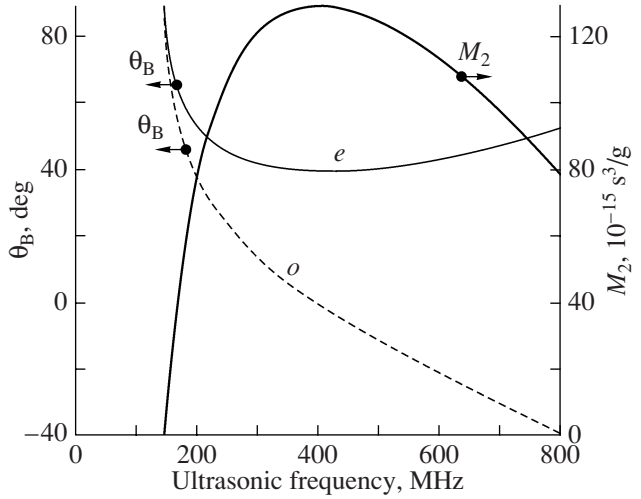

Fig. 3. Bragg angle θ_B and acoustooptic figure of merit M_2 vs. the ultrasonic frequency in the *XZ* plane. Ultrasound propagates at angle $\theta_a = 90°$.

The longitudinal and fast shear waves in the *XZ* plane of the crystal seem to be of minor applied interest because of a small value of M_2: for the longitudinal wave propagating along the *X* axis, M_2 does not exceed 23×10^{-15} s^3/g. This maximal value is achieved at collinear diffraction for $\lambda = 10.6$ μm and $f = 336$ MHz.

4.2. Acoustooptic Interaction in the YZ Plane

At anisotropic diffraction, acoustooptic figure of merit M_2 was shown to reach an absolute maximum in the *YZ* plane when the slow shear wave propagates along the direction given by $\theta_a = 108°$. This wave is polarized along the *X* axis, its velocity is $V_s = 1.11 \times 10^5$ cm/s, and the drift angle is $\alpha = 34°$ The diagram in Fig. 4 demonstrates the M_2 distribution when the optical wave diffracts by this (slow shear) wave. Its propagation direction is indicated by point *A*.

As follows from the calculation, M_2 here reaches a maximum of 160×10^{-15} s^3/g when the optical wave propagates at angles $\varphi_o = 90°$ and $\theta_o = 96°$. Thus, the maximal value of M_2 in the *YZ* plane is higher than in the *XZ* plane. Therefore, acoustooptic devices should employ acoustooptic interaction in the former plane. It also turned out that the acoustic frequency of matching, which corresponds to the maximal acoustooptic figure of merit in the crystal, is $f = 154$ MHz at $\lambda = 10.6$ μm. In the *Y* direction, diffraction may also be collinear. In this case, M_2 may reach a value of 100×10^{-15} s^3/g and diffraction is observed at ultrasonic frequency $f = 205$ MHz. The relatively high value of M_2 at collinear diffraction is due to the fact that the angle of propagation in this case, $\theta_o = 90°$, differs from optimal value $\theta_o = 96°$ (at which M_2 is maximal) only by several degrees.

More detailed information concerning the acoustooptic effect in the *YZ* plane can be gained from Fig. 5.

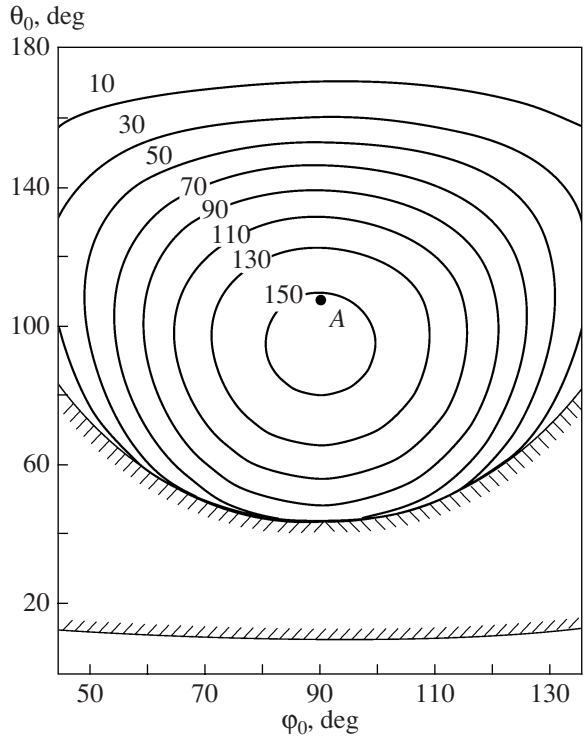

Fig. 4. Variation of the acoustooptic figure of merit with propagation direction of light in the *YZ* plane. Ultrasound propagated at angle $\theta_a = 108°$.

The continuous line shows the variation of the highest value of M_2 for various propagation directions of the shear acoustic wave, which are specified by angle θ_a. The respective Bragg angles are shown by the dashed line, and the dotted line shows the variation of the acoustic wave drift angle in the *YZ* plane. It is seen that the range of high M_2 correlates with the range of high Bragg angles in the *YZ* plane of tellurium. A strong drift of the acoustooptic energy in the *YZ* plane should be taken into consideration in the design of acoustooptic filters, since this phenomenon may cut the length of acoustooptic interaction. Accordingly, the diffraction efficiency and the spectral resolution of the filter may worsen.

It turned out that the maximal achievable value of the acoustooptic figure of merit under the conditions of anisotropic diffraction, $M_2 = 160 \times 10^{-15}$ s^3/g, is lower than $M_2 = 500 \times 10^{-15}$ s^3/g (the latter was predicted in [12]). This means that the data obtained in [12] are valid for only isotropic diffraction and cannot be extended for the case of anisotropic acoustooptic interaction. Nevertheless, the acoustooptic efficiency of tellurium crystals exceeds that of IR materials currently available even if diffraction proceeds under nonoptimal conditions.

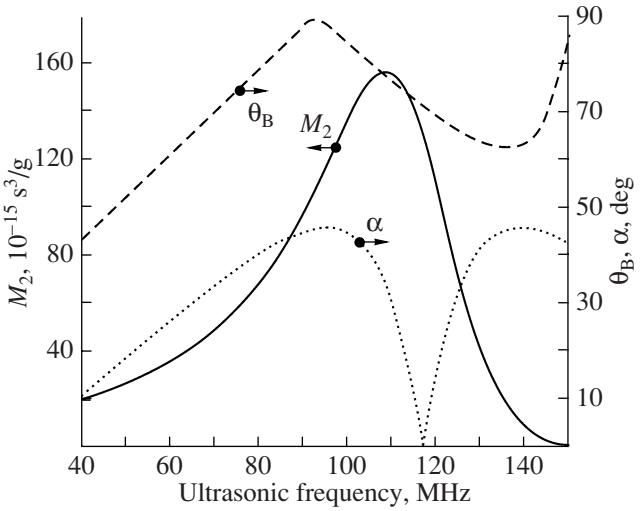

Fig. 5. Variation of the acoustooptic figure of merit M_2, Bragg angle θ_B, and acoustic wave drift angle α with propagation direction of ultrasound in the *YZ* plane of the crystal.

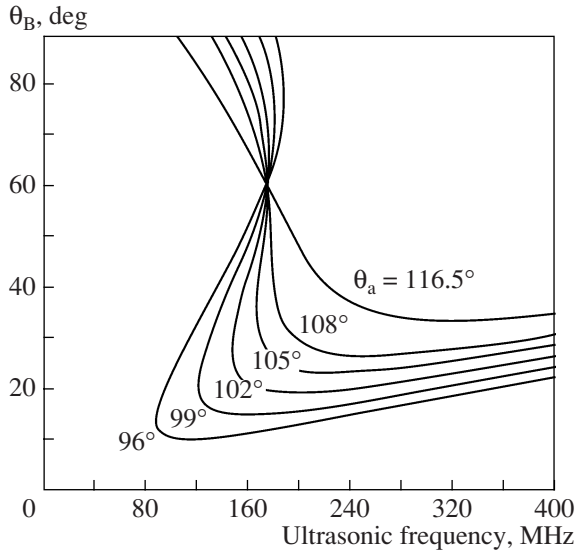

Fig. 6. Bragg angle vs. the ultrasonic frequency in the *YZ* plane for the wide-aperture geometry of acoustooptic interaction.

5. WIDE-APERTURE ACOUSTOOPTIC INTERACTION

It is known that a wide-aperture geometry of anisotropic diffraction is needed for control of uncollimated light and processing of images [1–4]. In the wide-angle regime, derivative $d\theta_B/df \longrightarrow \infty$ of function $\theta_B(f)$ tends to infinity. This fact imposes severe restrictions on angles at which light propagates in the crystal. Calculations show that wide-angle interaction in the *YZ* plane of tellurium is a possibility if the plane of electrooptic interaction is rotated through some angle about ultrasound vector **K**. One can also vary the direction of the slow shear wave, that is, angle θ_a, in the *YZ* plane. It was found that this angle can vary between 73° and 107°.

Figure 6 shows frequency dependences of the Bragg angle for the extraordinary incident optical wave and slow shear acoustic wave that propagates in the *YZ* plane. Angle θ_a is a parameter. Working regions in the domain of acoustooptic interaction are seen near the point where $d\theta_B/df \longrightarrow \infty$. By properly selecting the crystal cut, one can considerably displace these regions. However, the acoustooptic figure of merit in tellurium is high only if light propagates away from the optical axis. This is because coefficient p_{41} of the photoelasticity tensor is large, $p_{41} = 0.28$, compared with others; specifically, it is larger than coefficient $p_{44} = 0.14$, which can also provide anisotropic diffraction in the crystal [21].

The angles of sound and light propagation that satisfy the condition of wide-aperture interaction in the *YZ* plane are listed in the table. Each row corresponds to the conditions of anisotropic diffraction that do for image processing filters. The table includes ultrasound propagation angles θ_a, acoustic energy drift angles α, acoustooptic figures of merit M_2, velocities *V*, ultrasonic frequencies *f*, polar angles of light propagation θ_o, Bragg angles θ_B, and diffraction angles θ_d.

It should be noted that the wide-aperture conditions listed in the table are nonoptimal as far as the acous-

Acoustical, optical, and acoustooptic parameters of wide-aperture interaction in the *YZ* plane of tellurium

Acoustic polar angle, θ_a, deg	Acoustooptic drift angle α, deg	Phase velocity of sound *V*, 10^5 cm/s	Optical polar angle θ_o, deg	Bragg angle θ_B, deg	Diffraction angle θ_d, deg	Acoustooptic figure of merit M_2, 10^{-15} s^3/g	Ultrasonic frequency *f*, MHz
107	37	1.13	65	48	34.7	130	175
105	40	1.16	51	36	21.1	95	166
103	43	1.19	43	30	15.7	70	154
100	45	1.26	34.1	23.5	11	45	130
98	46	1.30	27	19	9	28	110
95	46	1.37	17	12	5	10	74
93	46	1.42	11	7.1	3	3	47

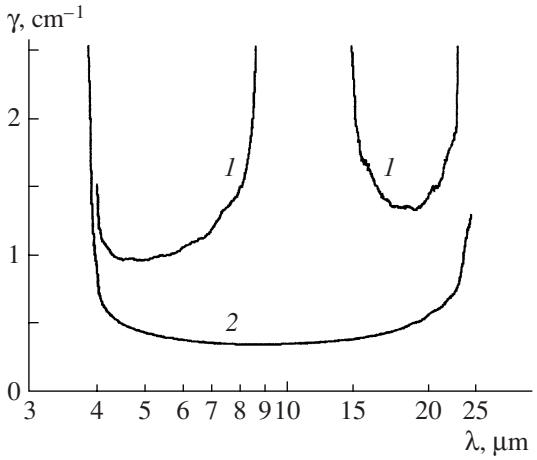

Fig. 7. Wavelength dependence of the optical absorption coefficient measured for the (*1*) extraordinarily and (*2*) ordinarily polarized light.

tooptic figure of merit is concerned. In general, the propagation direction of ultrasound in the filter and the Bragg angle should be selected with regard to requirements on the driving signal power and spectral resolution of the device. Such parameters as the optical transmission of the material, acoustic decay, etc., which determine the device performance, should also be considered in choosing the interaction geometry.

6. EXPERIMENTAL STUDY OF THE TELLURIUM OPTICAL PROPERTIES

Our experiments show that the acoustooptic interaction geometry in which light propagates away from the optical axis proves itself when the material is transparent for the infrared. It was found that the optical absorption in tellurium depends on several factors: purity of the seed, single crystal growth conditions, crystal lattice inhomogeneity, optical face finish, temperature, etc. [13, 14]. As has been noted above, Fresnel losses in uncoated samples of tellurium are extremely high because of a high refractive index, which decreases the luminous flux at the exit from the crystal. For example, the optical transmission of a thin tellurium ribbon under normal incidence is $T = 40\%$ for ordinarily polarized light and 30% for extraordinarily polarized light.

We measured optical power absorption coefficient γ of tellurium. Test samples were 0.4- and 1.2-cm-thick plane-parallel plates. They were cut parallel to the *X, Y,* and *Z* crystal axes. The transmission coefficient was measured in the mid- and far-IR ranges at wavelengths varying from 3 to 25 μm and also at a CO_2 laser wavelength of 10.6 μm. The measuring data are shown in Fig. 7 with allowance for reflection losses at the faces.

In the uncoated sample 1.2 cm long, the energy transmission for nonpolarized light at $\lambda = 10.6$ μm directed along the optical axis is only 20%. For extraordinarily polarized light propagating along the *Y* and *X* axes, the transmission is close to zero. This is confirmed by Fig. 7, which plots absorption coefficient γ against wavelength λ for extraordinarily and ordinarily polarized radiations. In the former case, the absorption coefficient exceeds 3 cm^{-1} in the wavelength interval 8–12 μm. Note, however, that the measurement accuracy in this interval was not high. Beyond this interval, the absorption of the extraordinarily polarized radiation falls into the range 2–3 cm^{-1}. For the ordinarily polarized IR radiation, absorption coefficient γ (which also characterizes the transparency of the crystal) is 0.5–0.7 cm^{-1}. Hence, tellurium samples 1.0–1.5 cm in size can be used in acoustooptic devices. In the wavelength range 4–8 μm, larger crystals seem to be appropriate. Finally, near $\lambda = 10$ μm, notch filters in which ordinarily polarized light alone is applied can be designed [28].

In one of the crystals, wide-aperture geometry of acoustooptic interaction was realized for the slow shear acoustic wave propagating in the *YZ* plane at angle $\theta_a = 80°$ to the *Y* axis. Under these conditions, the Bragg matching frequency was taken to be equal to $f = 181$ MHz at $\lambda = 10.6$ μm according the computational data. Ordinarily polarized light incident on the crystal propagated in the acoustooptic cell at Bragg angle $\theta_B = 12°$. The velocity of the acoustic wave in the material was $V_S = 1.7 \times 10^5$ cm/s. The diffraction efficiency in the cell depended on the angle of incidence of the radiation on the cell only slightly. This evidences that exactly wide-aperture acoustooptic interaction was observed in the experiment.

The acoustooptic figure of merit was no higher than $M_2 = 15 \times 10^{-15}$ $s^3/g \pm 20\%$, which was in satisfactory agreement with the computational results. Note that the crystal cuts studied in the experiment were much more inferior to optimal ones in acoustooptic figure of merit.

CONCLUSIONS

Our investigation shows that single-crystalline tellurium can basically be used in acoustooptic devices controlling the optical radiation parameters in the mid- and far-IR ranges. However, if light propagates away from the optical axis, tellurium cannot be applied at wavelengths between 8 and 12 μm because of a high absorption of extraordinarily polarized beams in this range. If the absorption is weak, tellurium crystals can well be used even if light propagates near the *Z* axis. Antireflection coatings and cooling can raise the intensity of luminous fluxes at the exit from the crystal.

Tellurium crystal cuts offering a high diffraction efficiency are yet less transparent for extraordinarily polarized optical radiation. Therefore, when designing acoustooptic devices, one should select cuts with a smaller acoustooptic figure of merit but higher optical transmission. The anisotropic diffraction conditions listed in the lower part of the table are preferable for tel-

lurium-based acoustooptic devices, such as wide-aperture filters.

ACKNOWLEDGMENTS

This work was supported by the CRDF, grant no. RUP1-1663-MO-06.

REFERENCES

1. V. I. Balakshii, V. N. Parygin, and L. E. Chirkov, *Physical Principles of Acousto-Optic* (Radio i Svyaz', Moscow, 1985) [in Russian].
2. J. P. Xu and R. Stroud, *Acousto-Optic Devices: Principles, Desing and Applications* (Wiley, New York, 1992).
3. A. Goutzoulis and D. Pape, *Design and Fabrication of Acousto-Optic Devices* (Dekker, New York, 1994).
4. N. Gupta, *Optical Engineer's Desk Reference*, Ed. by W. L. Wolfe (Optical Society of America, Washington, 2003).
5. N. Uchida and N. Niizeki, Proc. IEEE **61**, 1073 (1973).
6. R. W. Dixon, J. Appl. Phys. **38**, 5149 (1967).
7. I. M. Sil'vestrova, Ch. Barta, G. F. Dobrzhanskii, et al., Kristallografiya **20**, 1062 (1975) [Sov. Phys. Crystallogr. **20**, 649 (1975)].
8. J. D. Feichtner, M. Gottlieb, and J. J. Conroy, Appl. Phys. Lett. **34**, 1 (1979).
9. M. Gottlieb, A. Goutzoulis, and N. Singh, Opt. Eng. **31**, 2110 (1992).
10. D. Suhre, L. Taylor, and N. Melamed, Opt. Eng. **31**, 2118 (1992).
11. D. Suhre and E. Villa, Appl. Opt. **37**, 2340 (1998).
12. J. Oliveira and E. Adler, IEEE Trans. Ultrasonics Ferroelectrics Frequency Control. **34**, 86 (1987).
13. J. J. Loferski, Phys. Rev. **93**, 707 (1954).
14. R. S. Caldwell and H. Y. Fan, Phys. Rev. **114**, 664 (1959).
15. R. W. Dixon and A. N. Chester, Appl. Phys. Lett. **9**, 190 (1966).
16. M. I. Zusman, N. K. Maneshin, E. R. Mustel', and V. N. Parygin, Radiotekh. Elektron. (Moscow) **18**, 1203 (1973).
17. A. M. D'yakonov, Yu. V. Ilisavskii, and I. I. Farbshtein, Pis'ma Zh. Tekh. Fiz. **3**, 564 (1977) [Sov. Tech. Phys. Lett. **3**, 231 (1977)].
18. S. Fukuda, T. Shiosaki, and A. Kawabata. J. Appl. Phys. **50**, 3899 (1970).
19. A. M. D'yakonov, Yu. V. Ilisavskii, and E. Z. Yakhkind, Zh. Tekh. Fiz. **51**, 1494 (1981) [Sov. Phys. Tech. Phys. **26**, 856 (1981)].
20. P. N. Gorlei, N. Ya. Kushnir, and V. A. Shenderovskii, Ukr. Fiz. Zh. **34**, 102 (1989).
21. D. Souilhac, D. Billerey, and A. Gundjian, Appl. Opt. **28**, 3993 (1989).
22. D. Souilhac, D. Billerey, and A. Gundjian, Appl. Opt. **29**, 1798 (1990).
23. D. Souilhac and D. Billerey, Proc. SPIE **1723**, 162 (1990).
24. D. Souilhac and D. Billerey, Proc. SPIE **2312**, 212 (1993).
25. J. F. Nye *Physical Properties of Crystals: Their Representation by Tensors and Matrices* (Clarendon, Oxford, 1957; Mir, Moscow, 1967).
26. B. A. Auld, *Acoustic Field and Waves in Solids* (Krieger, New York, 1990).
27. T. A. Fjeldly and W. Richter, Phys. Status Solidi B **72**, 555 (1975).
28. V. E. Voloshinov, L. N. Magdich, and G. A. Knyazev, Vestn. Mosk. Univ., Ser. 3: Fiz., Astron., No. 4, 36 (2005).

Translated by V. Isaakyan